buildings

MDPI

Article

Rewelding Residual Stress of Fatigue Crack at U-Rib-to-Deck of an Orthotropic Steel Deck

Ji Qian [1,2], Shi-Jie Song [1], Lin-Qiang Zhou [1], Pei-Yun Zhang [1] and Zhen-Bo Xu [3,*]

[1] School of Civil Engineering, Chongqing Jiaotong University, Chongqing 400074, China; jiqian@cqjtu.edu.cn (J.Q.); songshijie411@163.com (S.-J.S.); 611220080025@mails.cqjtu.edu.cn (L.-Q.Z.); 18784418447@163.com (P.-Y.Z.)
[2] State Key Laboratory of Mountain Bridge and Tunnel Engineering, Chongqing Jiaotong University, Chongqing 400074, China
[3] College of Civil and Transportation Engineering, Hohai University, Nanjing 211100, China
* Correspondence: 622210970013@mails.cqjtu.edu.cn

Abstract: The orthotropic steel deck is a prevalent stiffening girder structure utilized in long-span cable-stayed bridges and suspension bridges. Nonetheless, the issue of fatigue cracking has persisted in in-service orthotropic steel decks, significantly impacting the longevity of bridges. This study examines the analysis of the distribution of residual stress during the rewelding process of a fatigue crack at the U-rib-to-deck-plate joint of an orthotropic steel bridge deck. Additionally, the impact of the initial welding and the stiffness of the boundary constraint on the residual stress field during rewelding is discussed. The findings indicate that the removal of the fatigue crack prior to rewelding alleviates the transverse residual stress caused by the initial welding. After undergoing the rewelding procedure, both the transverse residual stress and the longitudinal residual stress exhibited a significant stress peak. More precisely, the transverse tensile stress underwent a rise from 21 MPa to 385 MPa, while the longitudinal tensile stress experienced an increase from 345 MPa to 525 MPa. Furthermore, the range of tensile stress within the longitudinal residual distribution expanded by 88%. Moreover, the stress redistribution during the rewelding of the local fatigue crack varied depending on the constraints imposed on the steel bridge deck. Notably, the transverse residual stress increases by 40.6% when compared to the absence of constraints. The findings of this research offer valuable insights for the implementation of rewelding repair techniques on steel bridge decks, emphasizing the significance of considering the effects of residual stresses induced during the rewelding process.

Keywords: orthotropic steel bridge deck; residual stress; fatigue crack; rewelding repair; boundary constraint stiffness

Citation: Qian, J.; Song, S.-J.; Zhou, L.-Q.; Zhang, P.-Y.; Xu, Z.-B. Rewelding Residual Stress of Fatigue Crack at U-Rib-to-Deck of an Orthotropic Steel Deck. *Buildings* **2023**, *13*, 2515. https://doi.org/10.3390/buildings13102515

Academic Editor: Mohammad Adil Dar

Received: 2 August 2023
Revised: 13 September 2023
Accepted: 2 October 2023
Published: 4 October 2023

1. Introduction

The utilization of orthotropic steel bridge decks with closed U-shaped stiffening ribs (U-ribs) is prevalent in the construction of wide, flat steel box girder bridges. During the welding procedure of a steel bridge deck, non-uniform heating of its components leads to the development of thermal stresses. When the thermal stress exceeds the yield strength of the material, plastic deformation occurs in the welding area. During the subsequent cooling process, the constrained deformation of the welding zone by the surrounding area leads to the formation of residual stress within the component. This phenomenon, known as residual stress, has been extensively studied [1,2]. The presence of residual stress has the potential to diminish the ultimate capacity and fatigue strength of the structure [3,4]. Research has indicated that fatigue cracks commonly emerge at the weld connection between the deck plate and the U-rib under wheel load. Once a fatigue crack initiates, it propagates along the thickness direction of the deck plate and gradually extends through the pavement layer [5–7].

When fatigue cracks manifest in steel bridge decks, it becomes imperative to employ an appropriate treatment approach to mitigate crack propagation and prolong the lifespan of the structure. Presently, prevalent crack treatment methodologies encompass borehole crack arrest, adhesive bonding reinforcement, and rewelding repair [8–10]. Recent decades have witnessed extensive research on the repair parameters of borehole crack arrest and adhesive bonding reinforcement technology, aiming to delay crack growth by either eliminating the crack tip or enhancing the local capacity. Additionally, the evaluation of the fatigue performance of repaired structures has been conducted using these parameters [11–14]. Nevertheless, the existing body of research on rewelding repair technology remains inadequate, and the impact of rewelding residual stress on the fatigue behavior of a bridge deck remains ambiguous.

Many studies have investigated the residual stress and fatigue properties of fillet welds, particularly the initial fillet weld in this study, at the U-rib-to-deck-plate joint of an orthotropic steel bridge deck during its construction phase. Puymbroeck et al. [15], Chen et al. [16], and Zhao et al. [17] conducted an experimental study to measure the residual welding stress of U-rib stiffened deck plates. It should be noted that limitations such as measurement errors, variations in model size, and limited test data hinder the ability to establish a universal law. In light of the advancements in computer technology, numerical simulation of the welding process has gained significant popularity. Kainuma [18], Puymbroeck et al. [15], Xiong et al. [19], and Gu et al. [20] conducted a comprehensive investigation on the distribution of residual welding stress in orthotropic steel bridge decks. Their research has successfully validated the accuracy of numerical simulations through experimental analysis. Furthermore, these studies have examined the residual stress and fatigue behavior resulting from initial fillet weld welding while also assessing the influence of welding residual stress on the fatigue life of the bridge decks. This research focuses on the initial fillet weld residual stress and incorporates the distribution of rewelding residual stress during the fatigue crack rewelding process. At present, there exists a scarcity of research pertaining to the residual stress field that remains at the site of fatigue cracking, as well as the newly formed residual stress field resulting from the implementation of secondary welding techniques for fatigue crack repair.

Investigating the residual stress induced by rewelding in the repair of fatigue cracks presents a more intricate challenge, as the rewelding process is conducted under the influence of an initial stress field and subjected to a complex boundary constraint. The findings of previous studies on butt welds in stainless steel tubes indicate that the rewelding procedure has a notable impact on the distribution of axial residual stress in neighboring heat-affected zones [21]. A distinct inference can be drawn from these findings, which suggests that the alteration in transverse stress is more pronounced when compared to the welding of new components with less stringent constraints [22,23]. Moreover, previous studies have indicated a positive correlation between the length of the weld and the magnitude of the increase in transverse residual stress [24]. Edwards et al. [25] and Leggatt [26] carried out relevant studies on repair welding of high-strength steels using various research methods, with the aim of obtaining the optimal repair welding principles. Bouchard et al. [27] performed fatigue tests again on the repaired specimens (specimens of rib-to-deck welds and diaphragm-to-rib welds in steel bridge decks) and discussed the position and propagation of the new cracks to evaluate the efficacy of the repairs. The results indicated that new cracks occurred in the rewelded zone, and the fatigue life after rewelding was determined by the new weld. Consequently, further investigation into the distribution of residual stress in the rewelded zone and the fatigue life after rewelding was determined by the new weld.

This study focuses on investigating the prevalent fatigue crack that occurs at the U-rib-to-deck-plate joint of an orthotropic steel bridge deck. Initially, the residual stress of the initial fillet weld is examined through both finite element simulation and experimental methods. Subsequently, the process of crack removal and multi-layer rewelding is analyzed, and the impact of the initial stress field and the stiffness of the boundary constraint on the resulting residual stress field is discussed.

2. Rewelding Repair Method

As a result of the impact of fatigue cracking, the deck plate thickness of recently constructed steel bridges exceeds 16 mm. Conversely, existing long-span cable-stayed bridges and suspension bridges commonly employ deck plates 12 mm thick. A comprehensive investigation has revealed significant issues with fatigue cracking in these bridge decks, with the most severe occurrences observed at the intersection of the longitudinal rib and deck plate (Figure 1). The occurrence of fatigue cracks at the weld in the orthotropic bridge deck is primarily attributed to the presence of stress concentration and elevated residual stress levels induced during the welding process. The fatigue damage on the outer side of the welded joint between the longitudinal rib and the bridge deck is large. At this time, fatigue cracks easily occur on the weld between the roof and the longitudinal rib and extend to the bridge deck, while the roof measured inside the longitudinal rib does not have obvious cracks. Addressing the issue of fatigue cracking in steel bridge decks that are currently in use poses a significant challenge for the management and maintenance of expensive bridges. Among the various repair methods available, crack removal and rewelding offer prompt and cost-effective solutions. The rewelding repair process adheres to specific guidelines outlined in the German steel bridge deck repair procedure DVS 1709. This procedure encompasses several essential steps, including the elimination of existing cracks, thorough cleaning of the weld root, and subsequent rewelding, as illustrated in Figure 2. However, the process of repairing cracks through rewelding will inevitably result in the introduction of additional residual stress. This newly introduced residual stress interacts with the pre-existing residual stress, thereby forming an unknown residual stress field that impacts the fatigue performance of a repaired steel bridge deck. Consequently, it becomes imperative to conduct research on residual stress, taking into account both the initial welding residual stress and the residual stress resulting from rewelding, under various constraint conditions.

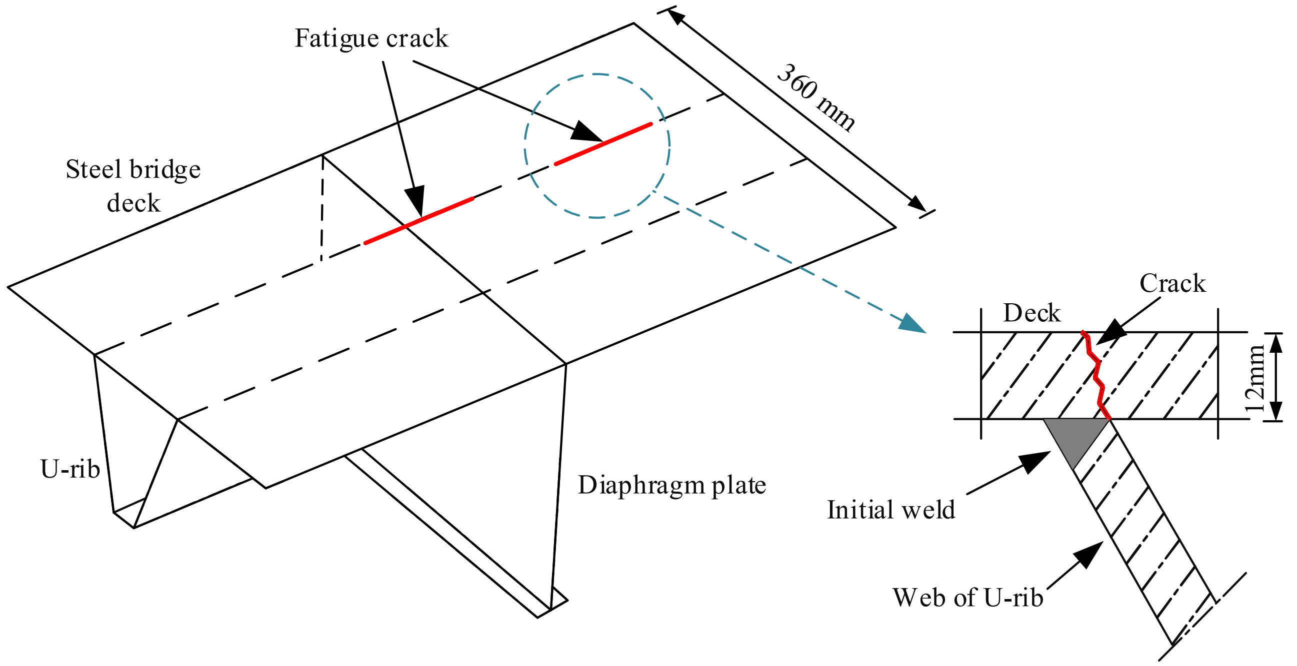

Figure 1. Fatigue crack at the U-rib-to-deck-plate joint of an orthotropic steel bridge deck.

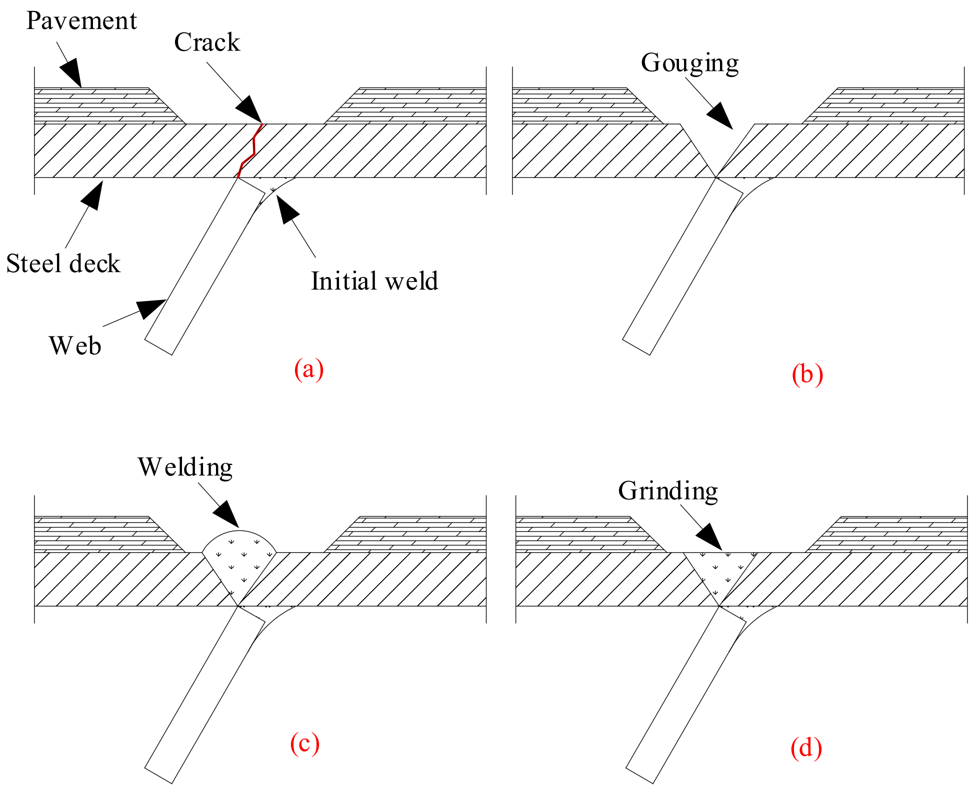

Figure 2. Rewelding repair procedure of cracks.

3. Finite Element Analysis of Rewelding Residual Stress

3.1. Geometric Model and Material Parameters

In this research, we analyze the structural form and the section geometry (as shown in Figure 3) of an orthotropic steel bridge deck, specifically focusing on the Sutong Yangtze Bridge, which holds the distinction of being the world's second-longest cable-stayed bridge. The analytical model utilized in this research has a length of 300 mm, and the material chosen for the bridge deck is Q345D low-alloy steel. For the sake of simplifying the analysis, it is assumed that the weld material is identical to the base metal. The material's parameters can be found in Table 1 [28].

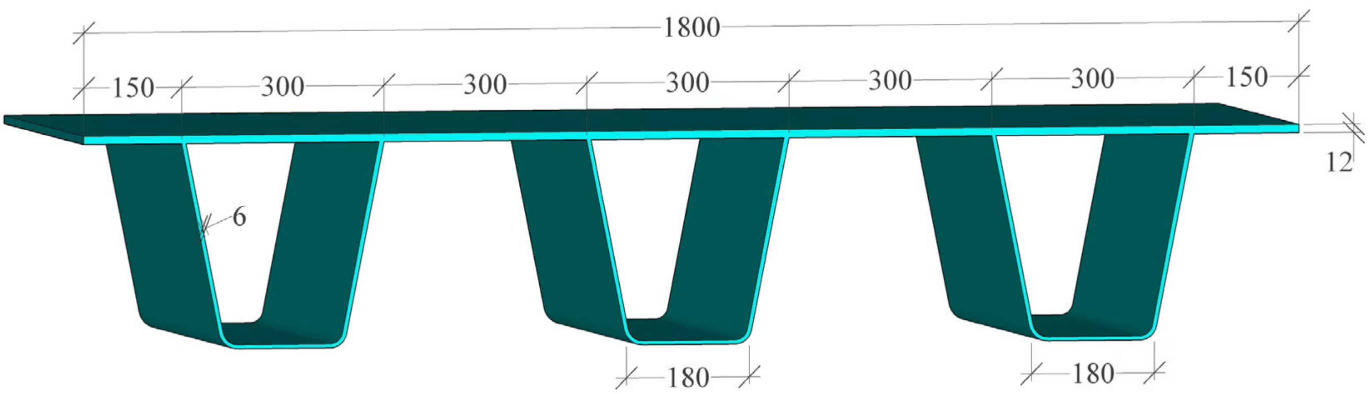

Figure 3. Geometric dimensions of steel bridge deck (mm).

Table 1. Mechanical properties of Q345D steel at different temperatures.

T/°C	Mechanical Properties of Q345D Steel			
	Yield Stress f/MPa	Elastic Modulus E/GPa	Poisson's Ratio ν	Coefficient of Thermal Expansion α
0	345.0	202	0.28	11.0
400	224.3	202	0.30	13.38
500	182.9	258	0.31	--
600	103.5	95	0.32	13.39
700	44.9	46	0.35	--
800	24.2	22	0.36	--
900	17.3	23	0.37	--
1000	10.4	8	0.38	--
1100	6.9	4	0.39	--
1200	0.0	0	0.40	20.05

In the course of welding, intricate physical and chemical reactions transpire within the weld pool, wherein each phenomenon interrelates, rendering comprehensive simulation of the welding process arduous. The objective of this study is to examine the temperature field engendered by welding and the consequent stress field. Consequently, the finite element simulation omits the consideration of influential factors like fluid dynamics and surface tension in the fluid state during welding, and instead relies on the following assumptions: (1) The chemical reaction, stirring, and flow phenomena occurring within the molten pool are disregarded. (2) A constant welding speed is employed. (3) Only unidirectional thermo-mechanical coupling is taken into account. Although the actual welding process involves thermal-stress coupling, the plastic deformation heat and latent heat generated by the specimen during welding are lower than the input welding heat. Consequently, it is assumed that the stress field does not impact the temperature field. In other words, only the unidirectional influence of the temperature field on the stress field is considered.

3.2. Finite Element Heat Source Model

The configuration of the welding heat source plays a crucial role in determining the energy distribution within the weld pool, thereby impacting the spatial variation of the welding temperature gradient. This, in turn, affects both the quasi-steady temperature field and the cooling temperature field. In order to achieve more precise results in finite element simulations of welding, it is recommended to employ a double ellipsoid heat source model. The Goldak double ellipsoid model [29] has been found to effectively depict the density distribution of the heat source during its forward progression. The double ellipsoid heat source model, which is frequently employed in gas-shielded welding and submerged arc welding processes, is utilized to describe the welding repair of the steel bridge deck. The specific double ellipsoid heat source model employed in this study is depicted in Figure 4.

The heat flux densities of the front and rear ellipsoids are determined through the following calculations [30]:

$$q_i(x,y,z) = \frac{6\sqrt{3}f_i\eta UI}{abc_i}\exp\left(-\frac{3x^2}{a^2} - \frac{3y^2}{b^2} - \frac{3z^2}{{c_i}^2}\right)\ i = 1,2 \quad (1)$$

where f_1, f_2 is the energy fraction of the front and rear hemispheres, and $f_1 + f_2 = 2$. η is heat input efficiency, U is voltage, I is current. c_1 and c_2 are the half lengths of the front and rear ellipsoids; a and b correspond to the width and depth of the heat source. q_1 and q_2 represent the heat input density before and after the molten pool (W/mm^3).

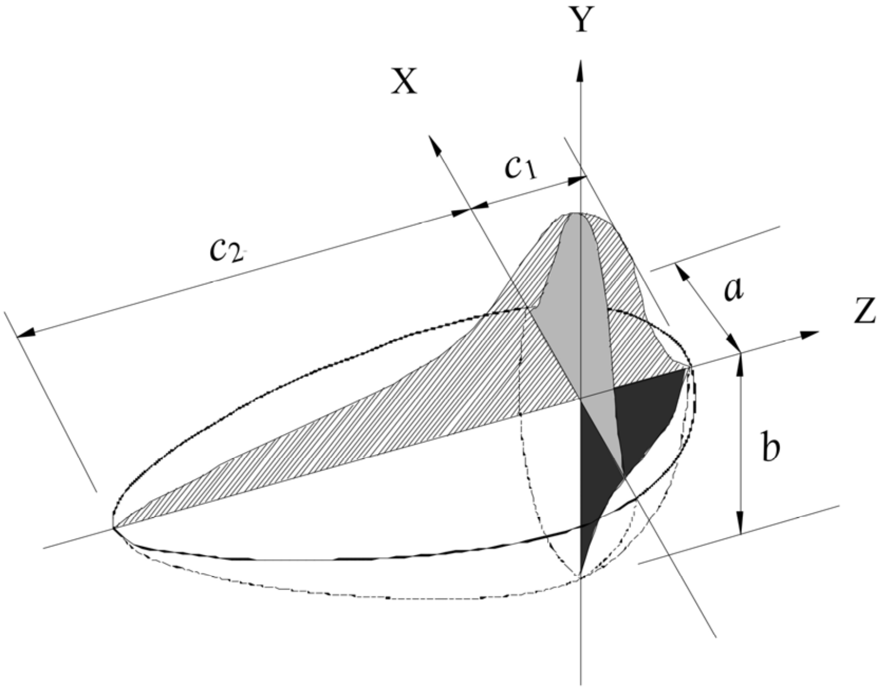

Figure 4. Double ellipsoid heat source model.

3.3. Initial Welding Stress Field

During crack rewelding, the presence of a residual stress field resulting from the initial welding around the crack is observed in contrast to the typical sequential welding process employed in construction. Shahani et al. [31] have demonstrated that the residual stress surrounding the crack is alleviated during the initiation and propagation of fatigue cracks. Generally, the initiation and propagation of cracks lead to the release of certain residual stresses. The removal of a crack and the subsequent formation of a V-shaped groove prior to rewelding facilitate the release of a portion of the residual stresses in the vicinity of the crack region. At present, a comprehensive elucidation regarding the persistence of stress after partial stress release and its impact on the rewelding procedure remains elusive. Consequently, this study endeavors to examine the effect of the residual stress field from an initial weld through the simulation of ANSYS finite element software.

To streamline the model, the U-rib's symmetry is exploited, typically involving the analysis of half of a U-rib, as depicted in Figure 5. The displacement boundary conditions of the finite element model are established to ensure that the free deformation of the welding process is not impeded. These conditions are based on the actual welding constraints and are designed to prevent rigid body displacement during the finite element calculation process. In the coordinate system of the finite element model, the X-direction represents the vertical weld, the Y-direction represents the deck thickness, and the Z-direction represents the weld length. The symmetric constraint is implemented along the symmetric centerline of the U-rib, whereby the displacement in the Y direction on both sides of the bottom surface of the deck plate is constrained to emulate the support platform. Conversely, the displacement in the Z direction is restrained on the opposite side of the deck plate.

The thermo-mechanical sequential coupling analysis method is employed to sequentially conduct thermal analysis and structural analysis. In the thermal analysis, the generation of the finite element model involves the utilization of the eight-node hexahedral thermal element (SOLID70), wherein only one degree of freedom is assigned for the temperature at each node. Conversely, in the Ansys analysis, due to the identical geometric shape shared by the thermal element (SOLID70) and the structural element (SOLID185), the thermal element (SOLID70) can be substituted directly with the corresponding structural element (SOLID185). The latter is an eight-node three-dimensional solid element that possesses three displacement degrees of freedom per node, thereby facilitating the creation of the structural finite element model.

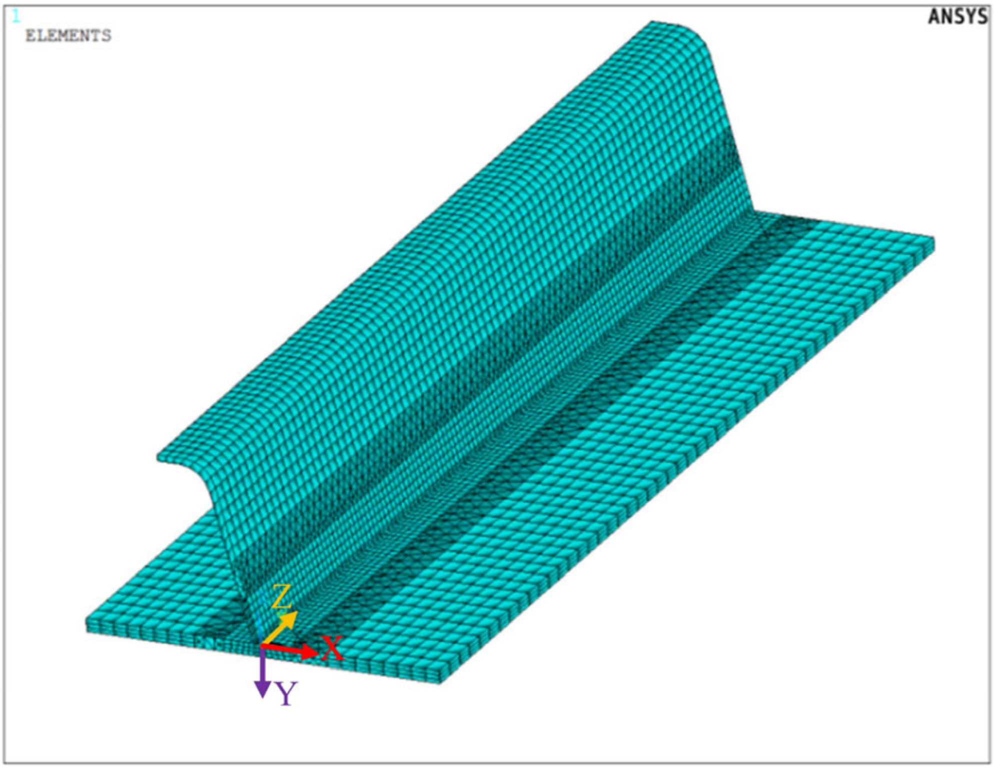

Figure 5. Model of finite element calculation.

The simulation of the fillet weld at the U-rib-to-deck-plate joint of an orthotropic steel bridge deck employs the double ellipsoid welding heat source as the input for welding heat. The parameters for the heat source, namely, a, b, c_1, and c_2, are determined as 0.008, 0.012, 0.012, and 0.048, respectively, while the initial temperature is set at 20 °C. Numerous research findings have been published on the residual stresses of a steel bridge deck calculated using the standard welding process [32,33]; thus, this paper does not delve into a detailed discussion of this matter. The resulting Mises equivalent residual stress after the initial weld cooling is shown in Figure 6.

As shown in Figure 7, the blind hole method was used to measure the residual stresses along the weld direction of the bridge deck after the initial weld cooling. The detailed test process and the data are shown in Reference [18]. Because the measuring points of each section were discontinuous due to the limitations of feasibility and cost, five measuring points were arranged along the measuring path. Hence, drawing upon the available literature and experimental findings, the analysis incorporated a line connecting each measuring point to account for the self-balancing nature of compressive/tensile residual stress and to visually represent the distribution of residual stress more effectively. Thus, the distribution can be reflected distinctly. A comparison between the measured data and the finite element data is shown in Figure 8.

The comparison between the yield strength of the deck plate and the maximum discrepancy of 5.2% observed in the finite element analysis results of the longitudinal residual tensile stress, as depicted in Figure 8, indicates that the measured longitudinal residual tensile stress aligned well with the numerical simulation outcomes. This finding underscores the accuracy of the employed finite element simulation approach in terms of predicting the welding residual stress.

Further, the removal of groove elements, as depicted in Figure 2, results in the creation of an empty welding channel to be rewelded based on the initial welding residual stress.

Subsequently, during the rewelding procedure, a portion of the stress is alleviated, leading to the formation of a residual stress field after redistribution. This field serves as the initial state for analyzing the stress evolution during the rewelding process.

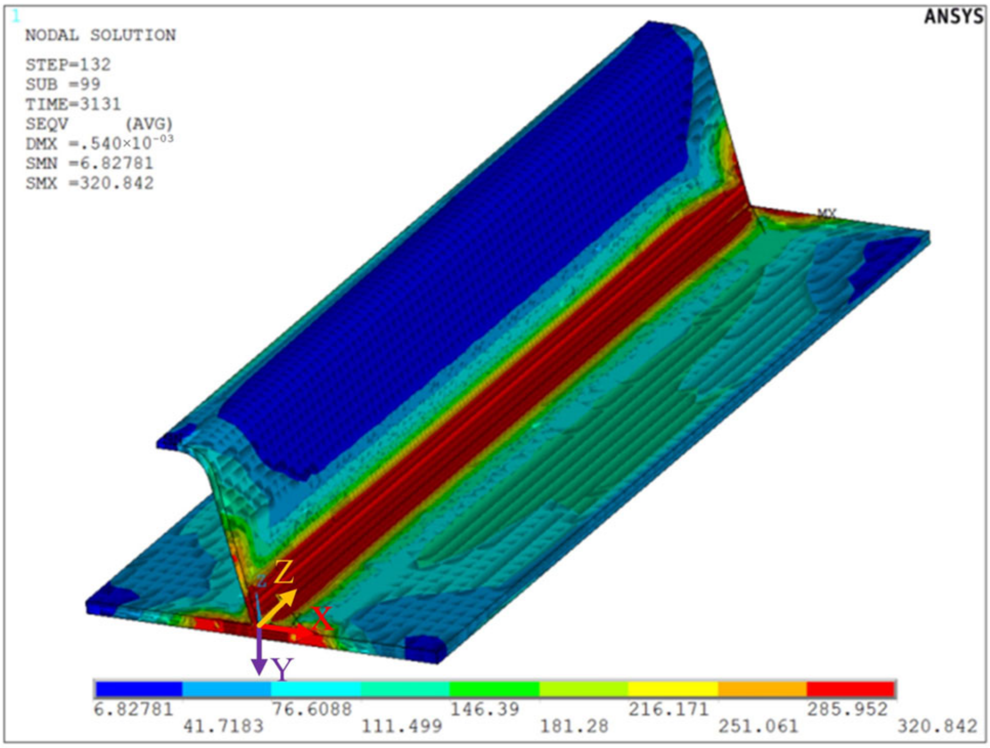

Figure 6. Mises equivalent stress field.

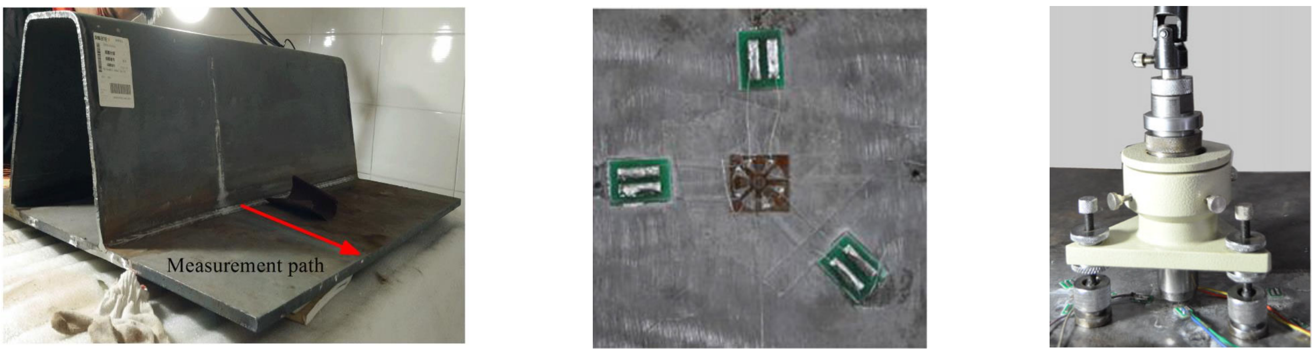

(**a**) (**b**) (**c**)

Figure 7. Test of the residual stress of steel bridge plate with the blind hole method. (**a**) Schematic diagram showing the measurement path; (**b**) strain rosette; (**c**) drilling.

3.4. Boundary Conditions of Rewelding

The formation of the reweld bead occurs after the removal of the pre-existing fatigue crack. Consequently, the boundary conditions for the rewelding process differ from those of the initial welding, necessitating consideration of the impact of the constraint stiffness of the deck surrounding the weld. Due to the greater bending stiffness of the longitudinal ribs in comparison to the deck plate, the stress experienced by the deck plate between the ribs is treated as that of a one-way plate. This is illustrated in Figure 9, where a segment of the deck with a unit width is selected in the direction of the longitudinal rib. Due to the requirement of the #2 rib exposing the groove at the crack location, rendering it no longer a closed section, its stiffness is disregarded. Given the substantial stiffness of the closed section, the #1 and #3 closed rib sections are established as fixed constraint boundary conditions. Consequently, the simplified constraint stiffness of the constraint conditions during the local welding of the #2 rib is computed. The elastic constraint boundary stiffness of the finite element model corresponds to the stiffness of the free end when the #1 and #3 longitudinal ribs are consolidated, as shown in Figure 9.

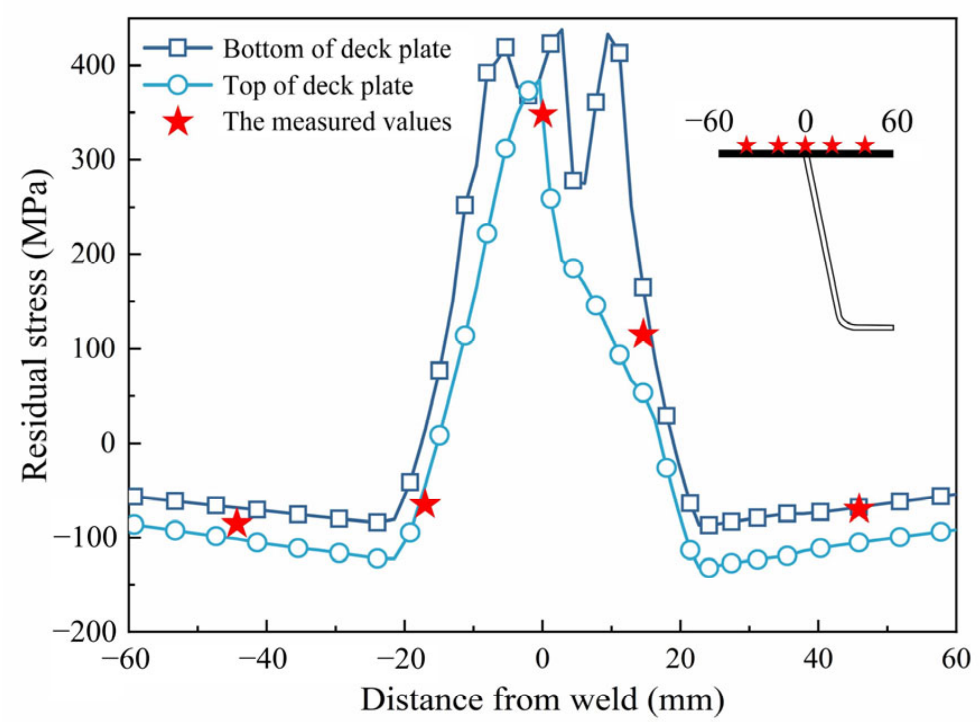

Figure 8. Comparison of the longitudinal residual stress of finite element and measured data.

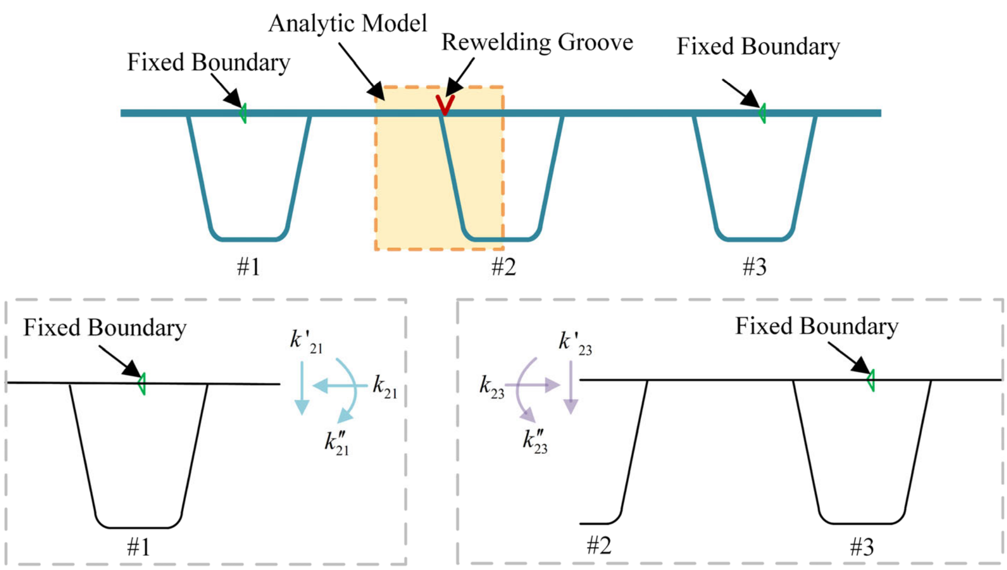

Figure 9. Diagram of weld elastic boundary calculation (mm).

The axial stiffnesses of the finite element model boundary restrained by the #1 rib and the #2 rib are:

$$k_{21} = EA/l_1,\ k_{23} = EA/l_3 \tag{2}$$

The shear stiffnesses of the finite element model boundary restrained by the #1 rib and the #2 rib are:

$$k'_{21} = GA,\ k'_{23} = GA \tag{3}$$

The bending stiffnesses of the finite element model boundary restrained by the #1 rib and the #2 rib are:

$$k''_{21} = EI/l_1,\ k''_{23} = EI/l_3 \tag{4}$$

where k_{21}, k'_{21}, and k''_{21} are the axial stiffness, shear stiffness, and bending stiffness of the model restrained by the #1 rib, respectively. k_{23}, k'_{23}, and k''_{23} are the axial stiffness, shear stiffness, and bending stiffness restrained by the #3 rib, respectively. E is Young's modulus, G is the shear modulus, I is the moment of inertia of the section, A is the cross-sectional area, l_1 is the distance from the #1 rib to the model boundary, and l_3 is the distance from the #3 rib to the model boundary.

4. Results and Discussion

4.1. Rewelding Temperature Field

The modeling approach for rewelding is analogous to that of the initial welding process, and the model was subjected to an equivalently simplified constraint condition. Initially, the birth–death element as eliminated, redirecting its heat flux to the node connecting the remaining model section and the removed area, thereby simulating the dissipation of residual stress in the groove region of the weld. Subsequently, the double ellipsoid heat source was incrementally shifted layer by layer, corresponding to the three layers of the weld, and the residual stress resulting from the rewelding process was computed through thermo-mechanical coupling. The dimensions of the weld zone mesh were 1 mm × 1 mm × 2 mm, comprising a total of 73,397 solid185 solid elements (Figure 10). The rewelding parameters remained consistent with those outlined in the preceding initial welding process.

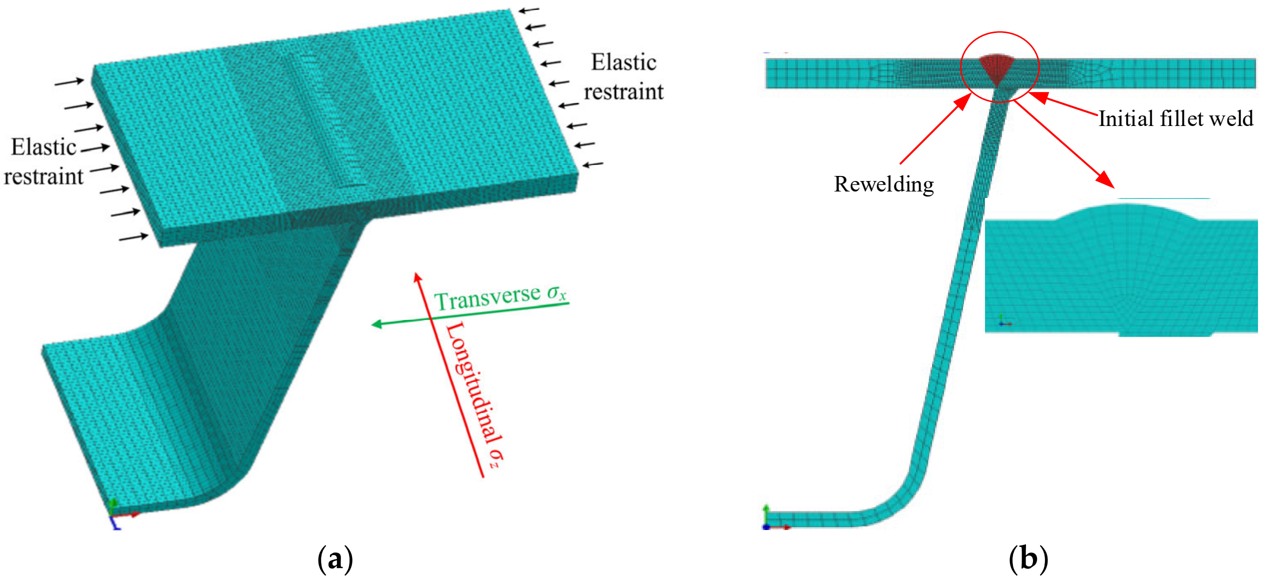

Figure 10. Meshing and constraint setting of finite element model. (**a**) Boundary constraint condition; (**b**) Position of welding.

Figure 11 depicts the temperature contours of the three-layer weld bead during the rewelding process. It can be observed that the central temperature of the weld pool exceeded 1550 °C, which aligns with the distribution characteristics. Specifically, the temperature field gradient of the double ellipsoid heat source intensified in the direction of its movement, while it noticeably diminished in the opposite direction. Moreover, the temperature field exhibited a symmetrical pattern along the weld direction and facilitated heat transfer towards the periphery.

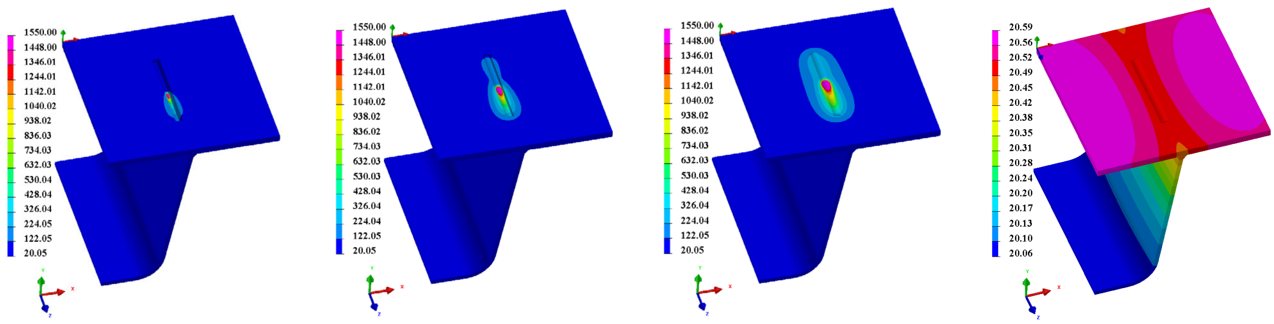

(**a**) (**b**) (**c**) (**d**)

Figure 11. Transient temperature field of rewelding (°C). (**a**) The heat source movement in the first bead; (**b**) the heat source movement in the second bead; (**c**) the heat source movement in the third bead; (**d**) temperature of U-rib at cooling.

Within an 8 cm vicinity surrounding the weld seam, three layers were chosen, with each layer consisting of five selected nodes. Consequently, a total of fifteen nodes were designated for the purpose of analyzing temporal fluctuations in temperature. The specific locations of these selected nodes are visually depicted in Figure 12. Subsequently, the temperature variations over time for each individual node were computed and are presented in Figure 13. The temperature field between the weld bead and the temperature changes of each node with time exhibited variations due to the welding time sequence and the filling of the weld bead. Nodes located on the same bead, such as A1–A5, experienced a delay in the arrival time of the peak temperature as the distance from the bead increased, accompanied by a rapid decrease in the peak temperature. Furthermore, notable disparities were found in the temperatures observed across different weld beads. The third weld bead attained a maximum temperature of 600 °C at the A bead nodes, whereas the first weld bead registered a maximum temperature below 200 °C at the C bead nodes. The heat conduction effect of weld filling resulted in a larger heat-affected zone in the cap weld.

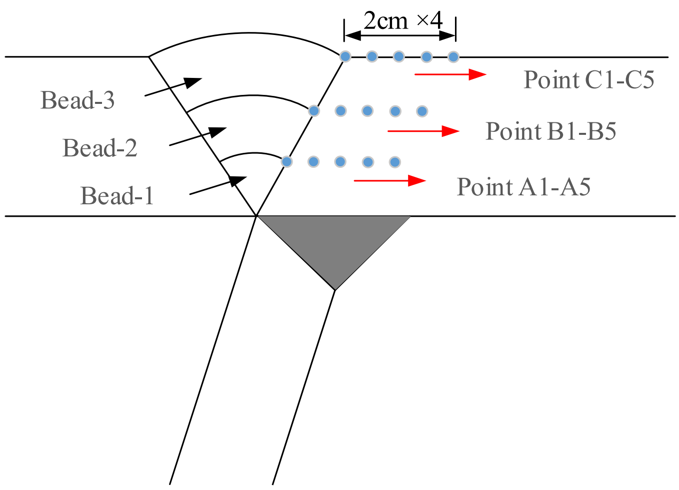

Figure 12. The position of the temperature analysis node (blue circles).

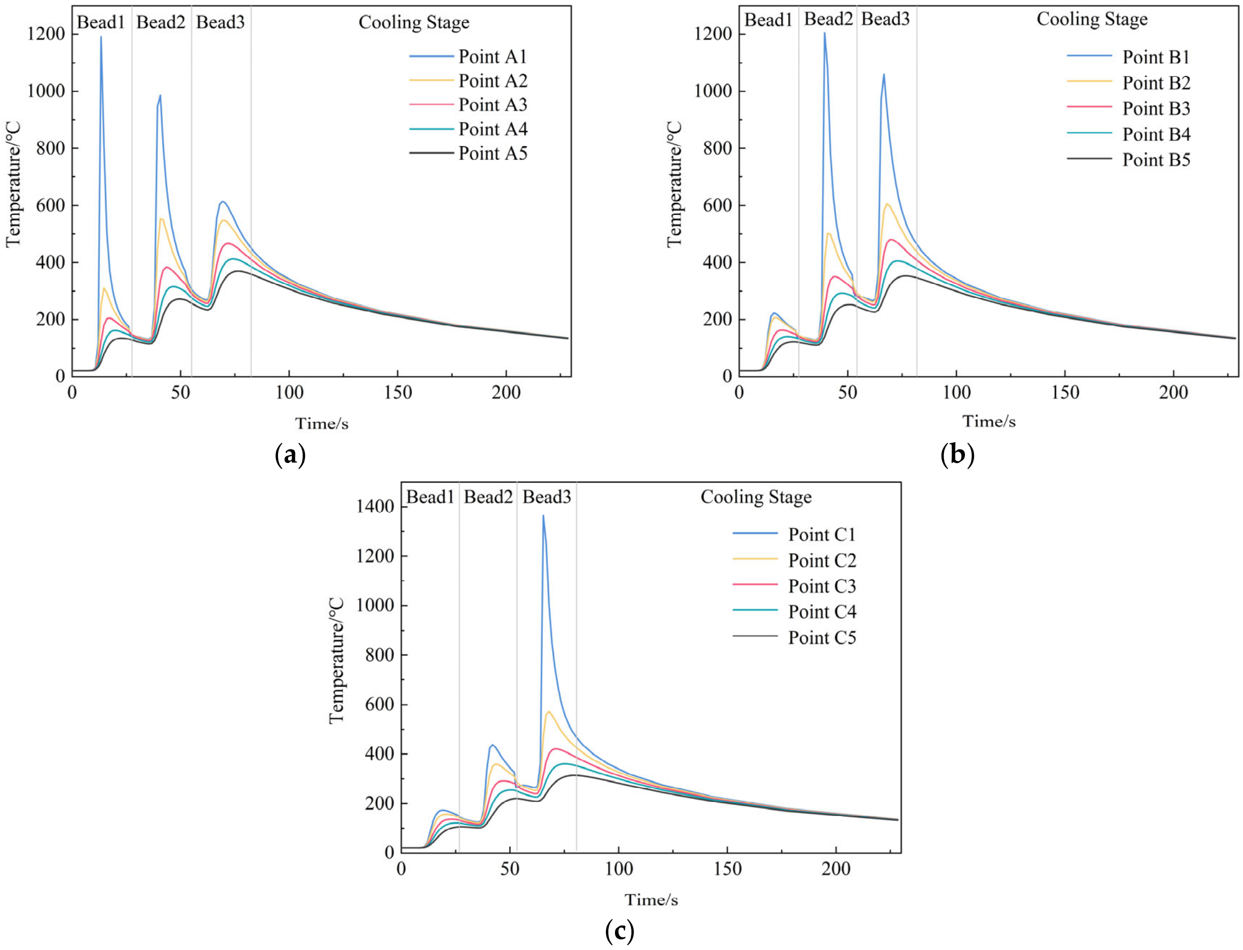

Figure 13. Diagrams of the temperature changes at different times. (**a**) Temperature variation curve of nodes A1–A5; (**b**) temperature variation curve of nodes B1–B5; (**c**) temperature variation curve of nodes C1–C5.

The temperature field was symmetrical in the center of the weld. During the welding procedure, the majority of the top and web components remained at ambient temperature. The application of high-density energy resulted in a significant disparity in temperature between the weld and the base metal region. Consequently, the material within the weld area experienced varying degrees of constraint from the base metal during the expansion and contraction phases of heating and cooling. This phenomenon plays a pivotal role in determining residual distribution.

4.2. Rewelding Residual Stress

Rewelding repairs involve conducting welding repairs after the creation of a groove on the top plate. The welding seam undergoes inherent constraints from the adjacent material during the heating and cooling procedure. As a result, the welding residual stress that arises upon cooling to ambient temperature will differ from the stress distribution observed during the initial fillet weld processing. The temperature field obtained from the thermo-mechanical analysis of rewelding through sequential coupling is presented in Figure 11, whereas the residual stress field is depicted in Figure 14.

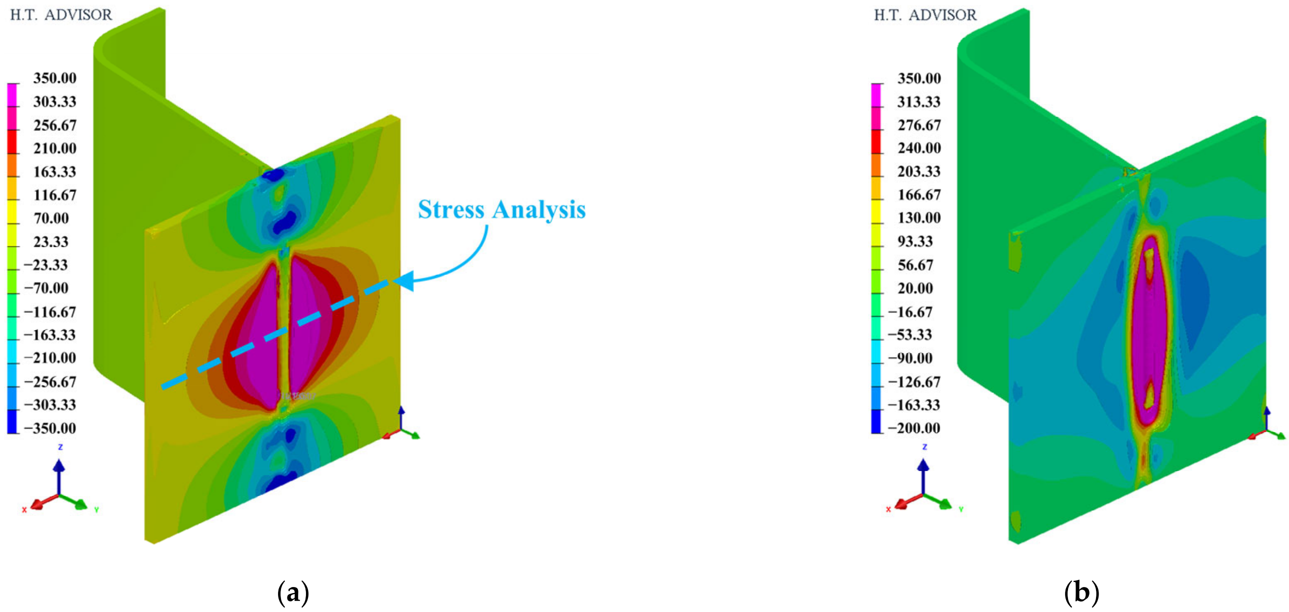

Figure 14. Distribution of residual stress field (MPa). (**a**) Transverse residual stress; (**b**) longitudinal residual stress.

Figure 14 depicts the residual stress field of the weld after cooling, taking into account the initial stress and elastic boundary constraints. The welding process imposed a robust constraint around the deck, resulting in the persistence of longitudinal tensile stress of approximately 80 MPa at the deck's edge. This disparity in residual stress distribution between the rewelded deck and the free boundary deck under initial construction conditions was substantial.

In order to assess the variations in residual stress throughout the entirety of the rewelding process, the stress analysis was partitioned into three distinct stages based on the aforementioned rewelding repair procedure. The initial stage involved the creation of a primary weld, the residual stress of which is examined in Section 3.3. Subsequently, in the second stage, the fatigue crack was eliminated and a rewelding groove was established, resulting in the partial release of the residual stress accumulated in the preceding stage. The residual stress subsequent to crack removal is visually depicted in Figure 15. The residual stress analysis in this study involved the examination of transverse and longitudinal residual stresses. The orange line in the graph represents the transverse residual stress, whereas the brown line represents the longitudinal residual stress during the initial stage. The second and third stages of the analysis encompassed initial residual stress and boundary constraints. Figure 15 illustrates the residual stress that arose from the rewelding process. The transverse residual stress of beveling is represented by the pink line, while the blue line represents the longitudinal residual stress of beveling. Furthermore, the red line signifies the transverse residual stress of reweld, and the purple line represents the longitudinal residual stress of the reweld. The positions of the stress analysis node in Figure 14 can be described in the following manner. A 300 mm long straight line was selected along the vertical weld direction, specifically in the middle of the weld length direction. The nodes located on this line were designated as stress analysis nodes, as depicted in Figure 14a.

First, the influence of the beveling on the initial weld stress field was analyzed. It should be emphasized that the stress field that formed after beveling is the initial residual stress in the rewelding calculation. Following the process of beveling, a significant alteration in the transverse stress (the orange line) adjacent to the weld region was observed, in contrast to the initial transverse stress (the pink line). This discrepancy suggests a substantial release of transverse stress predominantly in the vertical direction of the groove. The longitudinal stress (yellow line) did not change much compared with Figure 8, suggesting that the stress along the direction of the groove is less affected in the beveling process.

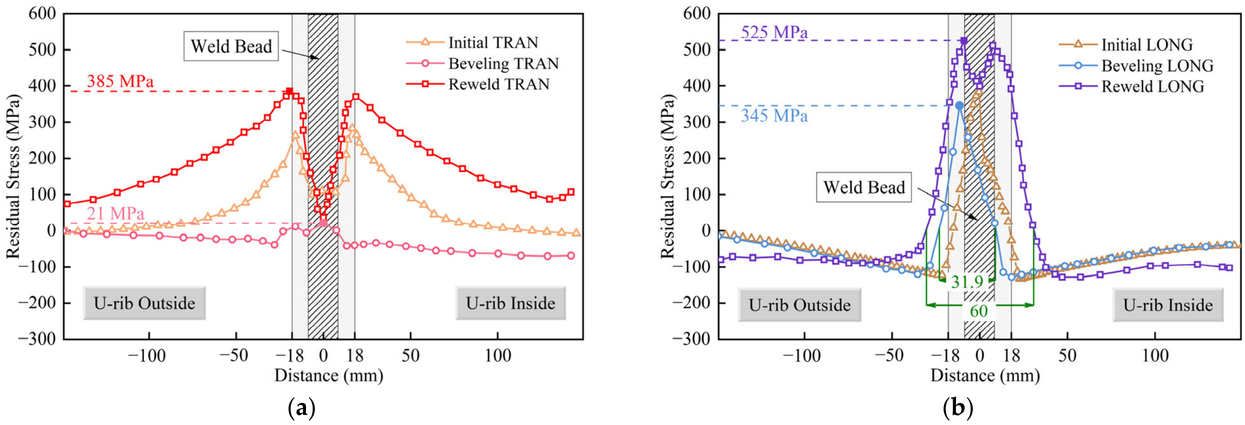

Figure 15. Residual stress distribution before and after rewelding on the upper surface of the deck. (**a**) Transverse residual stress; (**b**) longitudinal residual stress.

The residual stress field after rewelding is further analyzed. After rewelding, there is significant residual stress in both the longitudinal and transverse directions. However, the longitudinal residual stress (purple line) is higher than the transverse residual stress (red line) because the longitudinal residual stress was not fully released before rewelding, while the transverse residual stress was released more. However, the transverse residual stress increased more during rewelding. Compared with the residual stress generated by the beveling during construction, the residual longitudinal tensile stress in rewelding was higher than the yield strength in the range of about 18 mm from the centerline of the weld. The peak value of the tensile stress increased from 345 MPa to 525 MPa, and the distribution width of the tensile stress increased from 31.9 mm to 60 mm, with an increase of 88%. Meanwhile, the peak value of the transverse tensile stress in rewelding increased from 21 MPa to 385 MPa. In general, the transverse residual stress changes more obviously in rewelding, while the peak value and the influence range of longitudinal residual stress increased further. Therefore, the rewelding process should consider effective residual stress elimination measures.

During the rewelding cooling process, martensitic transformation occurred when the weld bead pool temperature was lower than the martensitic temperature. The volume expansion caused by the transformation was much greater than the thermal strain caused by austenite cooling. The solid phase transformation produced compressive stress in the hot melt pool area, thus greatly reducing the tensile stress in the weld pool position, as shown in Figure 15.

4.3. Influence of Boundary Constraints

In the determination of the initial weld residual stress for a steel bridge deck, it is customary to employ a calculation model that is statically determined in its entirety, disregarding the impact of boundary conditions. Nevertheless, the rewelding procedure entails partial welding across the entire bridge deck, and neglecting the boundary constraints will yield imprecise calculation outcomes. To examine the effect of boundary conditions on the residual stress resulting from rewelding, four distinct boundary constraints are taken into account. The four types of boundaries considered in this study include the free boundary, the boundary with solely axial constraints, the boundary with both axial and tangential constraints, and the fully constrained boundary. In the preceding calculation, the axial and tangential elastic constraints were employed. The longitudinal and transverse residual stress distributions for each of the four boundary conditions are presented in Figure 16.

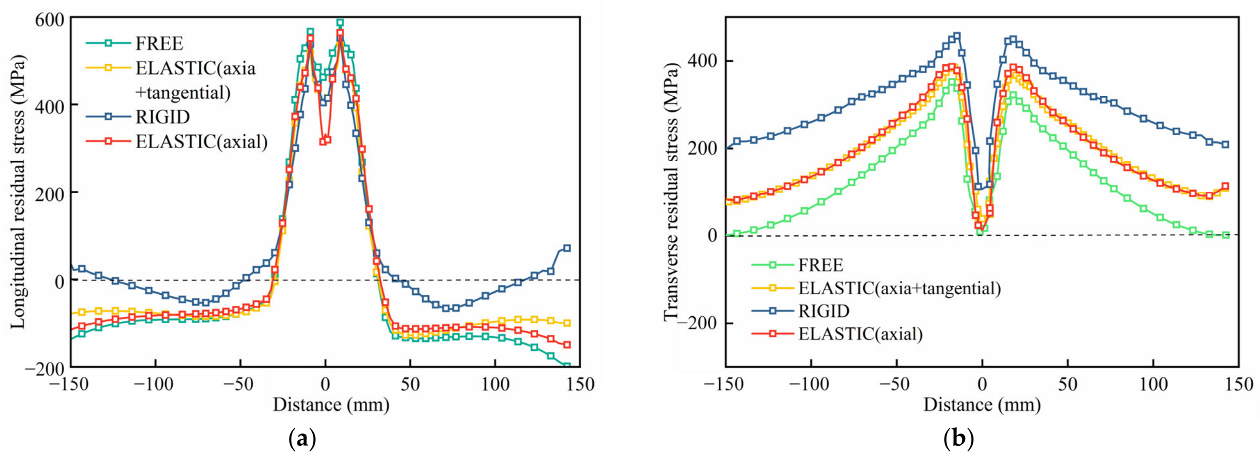

Figure 16. Comparison of rewelding residual stress for different constraints. (**a**) Longitudinal residual stress with four boundary constraints; (**b**) transverse residual stress with four boundary constraints.

The longitudinal residual stress near the heat-affected zone was minimally influenced by the boundary constraint, as depicted in Figure 16a, while the compressive stress at the model's edge was affected. When a fully constrained boundary was imposed, tensile stress was observed at the model's edge. Comparatively, the transverse residual stresses were more influenced by the boundary conditions. Figure 16b illustrates a similar distribution of transverse residual stress under different boundary conditions. The maximum tensile stress experienced a 40.6% increase, rising from 320 MPa to 450 MPa, as the stiffness of the boundary constraint increased. Additionally, the tensile stress at the edge position increased from 0 MPa to 200 MPa. It is important to acknowledge that the elastic constraint boundary utilized in this study yielded simplified calculation outcomes, with the constraint stiffness falling between that of a free boundary and a fully constrained boundary. The calculation results depicted in Figure 16 demonstrate that the residual stress lies within the range of the free boundary and the fully constrained boundary, thereby indicating the reasonableness of the obtained results.

Typically, the transverse residual stress arising from the elastic constraint lies within the range of the free boundary and the fully constrained boundary. Consequently, when assessing fatigue strength after rewelding, it is imperative to account for the impact of boundary constraints in order to attain more precise outcomes and prevent the underestimation of the influence of residual stress by employing free boundary conditions.

5. Conclusions

The rewelding repair technology offers a convenient and efficient solution for addressing longitudinal fatigue cracks occurring at the U-rib-to-deck-plate joint of an orthotropic steel bridge deck. It should be noted that this repair process inevitably generates new residual stresses, which exhibit distinct characteristics compared to the original weld. During the removal of the fatigue crack prior to rewelding, a partial release of the residual stress from the original weld occurred. The findings of the analysis indicate that the transverse residual stress in the vicinity of the beveling zone was effectively alleviated, whereas the longitudinal residual stress remained relatively stable. Upon completion of the rewelding process, significant transverse residual stress was anticipated, with a peak value approaching the initial transverse residual stress. In comparison to the residual stress induced by the initial welding process during construction, the residual longitudinal tensile stress in rewelding surpassed the yield strength within a span of approximately 18 mm from the weld's centerline. The peak value of the residual tensile stress escalated from 345 MPa to 525 MPa, while the distribution width of the residual tensile stress expanded from 31.9 mm to 60 mm, signifying an 88% increase. And the peak value of the transverse tensile stress in rewelding increased from 21 MPa to 385 MPa.

There was minimal disparity observed in the longitudinal tensile stress within the heat-affected zone across various boundary conditions. It should be noted that distinct variation is evident in the longitudinal compressive stress at the periphery of the model. When a fully constrained boundary was employed, tensile stresses were even observed at the model's edge. In relative terms, the transverse stress was more susceptible to alterations in the boundary conditions. In comparison to the free boundary condition, the tensile stress escalated from 320 MPa to 450 MPa when a fully constrained boundary was implemented. The present study employed an elastic constraint boundary condition lying between the free boundary condition and the rigid boundary condition. It is imperative to ensure that all actual conditions fall within this range. Consequently, when evaluating the fatigue strength following rewelding, it is crucial to account for the impact of boundary constraints and the initial welding stress field. This consideration is necessary in order to attain more precise outcomes and prevent the underestimation of the influence of residual welding stress, which may occur due to the simplification of assuming no initial stress field and free boundary conditions.

Author Contributions: Conceptualization, J.Q. and Z.-B.X.; methodology, S.-J.S.; software, L.-Q.Z.; validation, P.-Y.Z., S.-J.S. and L.-Q.Z.; formal analysis, S.-J.S.; investigation, L.-Q.Z.; resources, P.-Y.Z.; data curation, Z.-B.X.; writing—original draft preparation, Z.-B.X.; writing—review and editing, S.-J.S.; visualization, L.-Q.Z.; supervision, J.Q.; project administration, J.Q.; funding acquisition, J.Q. All authors have read and agreed to the published version of the manuscript.

Funding: This work was supported by the National Natural Science Foundation of China (Grant No. 52378283); China Postdoctoral Science Foundation (Grant No. 2021M702782); Natural Science Foundation of Chongqing, China (Grant No. CSTB2023NSCQ-MSX0633); Team Building Project for Graduate Tutors in Chongqing (Grant No. JDDSTD2022003).

Data Availability Statement: The data supporting the article's findings are available from the corresponding author upon reasonable request.

Conflicts of Interest: The authors declared no potential conflict of interest with respect to the research, authorship, and/or publication of this article.

References

1. Wang, Q.D.; Ji, B.H.; Fu, Z.Q.; Ye, Z. Effect of crack-closure treatment on fatigue durability of cracked rib-to-deck welded joints in steel bridge decks. *J. Cent. South Univ.* **2019**, *26*, 2554–2568. [CrossRef]
2. Liu, L.; Sun, J.; Chen, W.; Sun, P. Modified Layer-Removal Method for Measurement of Residual Stress in Pre-stretched Aluminium Alloy Plate. *J. Harbin Inst. Technol.* **2015**, *22*, 34–40.
3. Krebs, J.; Kassner, M. Influence of welding residual stresses on fatigue design of welded joints and components. *Weld. World* **2007**, *51*, 54–68. [CrossRef]
4. Zhang, Z.N.; Zhang, Y.C. Effects of welding residual stresses on the stability capacity of the monosymmetric I-beams. *J. Harbin Inst. Technol.* **2007**, *39*, 1864–1868.
5. Wang, Q.; Ji, B.; Li, C.; Zhongqiu, F. Fatigue evaluation of rib-deck welds: Crack-propagation-life predictive model and parametric analysis. *J. Constr. Steel Res.* **2020**, *173*, 106248. [CrossRef]
6. Yong, Z.; Yu, Q.; Anbang, G. Large sectional fatigue experiment of the orthotropic steel deck from a box-girder suspension bridge. *J. Harbin Inst. Technol.* **2016**, *48*, 95–100.
7. Aljabar, N.J.; Zhao, X.L.; Al-Mahaidi, R.; Ghafoori, E.; Motavalli, M.; Powers, N. Effect of crack orientation on fatigue behavior of CFRP-strengthened steel plates. *Compos. Struct.* **2016**, *152*, 295–305. [CrossRef]
8. Zhong-Qiu, F.U.; Bo-Hai, J.I.; Shu-Hui, X.; Liu, T.-J. Crack stop holes in steel bridge decks: Drilling method and effects. *J. Cent. South Univ.* **2017**, *24*, 2372–2381.
9. Yuan, Y.; Wu, C.; Jiang, X. Experimental study on the fatigue behavior of the orthotropic steel deck rehabilitated by UHPC overlay. *J. Constr. Steel Res.* **2019**, *157*, 1–9. [CrossRef]
10. Kim, Y.J.; Harries, K.A. Fatigue behavior of damaged steel beams repaired with CFRP strips. *Eng. Struct.* **2011**, *33*, 1491–1502. [CrossRef]
11. Ishikawa, T.; Shimizu, M.; Tomo, H.; Kawano, H.; Yamada, K. Effect of compression overload on fatigue strength improvedby ICR treatment. *Int. J. Steel Struct.* **2013**, *13*, 175–181. [CrossRef]
12. Kuhlmann, U.; Bove, S.; Hubmann, M. Instandsetzung und Verstärkung von Stahlbrücken mit Kategorie-2-Schäden. *Stahlbau* **2017**, *86*, 574–586. [CrossRef]

13. Stranghöner, N.; Lorenz, C.; Friedrich, H. Instandsetzung und Verstärkung von Stahlbrücken mit Kategorie-1-Schäden. *Stahlbau* **2017**, *86*, 562–573. [CrossRef]
14. Freitas, S.T.; Kolstein, H.; Bijlaard, F. Fatigue behavior of bonded and sandwich systems for strengthening orthotropic bridge decks. *Compos. Struct.* **2013**, *97*, 117–128. [CrossRef]
15. Puymbroeck, E.V.; Staen, G.V.; Iqbal, N.; De Backer, H. Residual weld stresses in stiffener-to-deck plate weld of an orthotropic steel deck. *J. Constr. Steel Res.* **2019**, *159*, 534–547. [CrossRef]
16. Chen, S.J.; Yang, K.C. Inelastic behavior of orthotropic steel deck stiffened by U-shaped stiffeners. *Thin-Walled Struct.* **2002**, *40*, 537–553. [CrossRef]
17. Zhao, Q.; Guo, Z.; Shen, X.; Briseghella, B. Test study on residual stress distribution of hybrid steel u-rib stiffened plates. *J. Constr. Steel Res.* **2016**, *121*, 261–267. [CrossRef]
18. Kainuma, S.; Jeong, Y.S.; Yang, M.; Inokuchi, S. Welding residual stress in roots between deck plate and U-rib in orthotropic steel decks. *Measurement* **2016**, *92*, 475–482. [CrossRef]
19. Xiong, Y.; Li, C.; Chen, Z.Y.; He, J.; Xin, H. The Evolution of Residual Stress in Rib-Diaphragm Joints of Orthotropic Steel Decks Subjected to Thermal Cutting and Welding. *Materials* **2020**, *13*, 3804. [CrossRef]
20. Gu, Y.; Li, Y.; Zhou, Z.; Ren, S.; Kong, C. Numerical Simulation and Measurement of Welding Residual Stresses in Orthotropic Steel Decks Stiffened with U-Shaped Ribs. *Int. J. Steel Struct.* **2020**, *20*, 856–869. [CrossRef]
21. Dong, P.; Hong, J.K.; Bouchard, P.J. Analysis of residual stresses at weld repairs. *Int. J. Press. Vessel. Pip.* **2005**, *82*, 258–269. [CrossRef]
22. Chen, Z.; Duan, Y.; Wang, P.; Qian, H. Residual Stress Redistribution Analysis in the Repair Welding of AA6082-T6 Aluminum Alloy Joints: Experiment and Simulation. *Materials* **2022**, *15*, 6399. [CrossRef] [PubMed]
23. Jiang, W.; Luo, Y.; Zeng, Q.; Wang, J.; Tu, S.T. Residual stresses evolution during strip clad welding, post welding heat treatment and repair welding for a large pressure vessel. *Int. J. Press. Vessel. Pip.* **2021**, *189*, 104259. [CrossRef]
24. Fu, Z.; Wang, Q.; Ji, B.; Yuanzhou, Z. Rewelding repair effects on fatigue cracks in steel bridge deck welds. *J. Perform. Constr. Facil.* **2017**, *31*, 04017094. [CrossRef]
25. Edwards, L.; Bouchard, P.J.; Dutta, M.; Wang, D.Q.; Santisteban, J.R.; Hiller, S.; Fitzpatrick, M.E. Direct measurement of the residual stresses near a 'boat-shaped' repair in a 20 mm thick stainless steel tube butt weld. *Int. J. Press. Vessel. Pip.* **2005**, *82*, 288–298. [CrossRef]
26. Leggatt, R.H. Residual stresses in welded structures. *Int. J. Press. Vessel. Pip.* **2008**, *85*, 144–151. [CrossRef]
27. Bouchard, P.J.; George, D.; Santisteban, J.R.; Bruno, G.; Dutta, M.; Edwards, L.; Kingston, E.; Smith, D.J. Measurement of the residual stresses in a stainless steel pipe girth weld containing long and short repairs. *Int. J. Press. Vessel. Pip.* **2005**, *82*, 299–310. [CrossRef]
28. *CEN, DAFT ENV 1993*; Eurocode 3: Design of Steel Structure. European Committee for Standardization: Brussels, Belgium, 1995.
29. Goldak, J.; Chakravarti, A.; Bibby, M. A new finite element model for welding heat sources. *Metall. Trans. B* **1984**, *15*, 299–305. [CrossRef]
30. Glickstein, S.S.; Friedman, E. Characterization and modeling of the heat source. In *ASM Handbook*; ASM International: Almere, The Netherlands, 1994; pp. 6710–6736.
31. Shahani, A.R.; Shakeri, I.; Rans, C.D. Effect of residual stress redistribution and weld reinforcement geometry on fatigue crack growth of butt welded joints. *Int. J. Fatigue* **2020**, *139*, 105780. [CrossRef]
32. Wang, F.; Lyu, Z.D.; Zhao, Z.; Chen, Q.-K.; Mei, H.-L. Experimental and numerical study on welding residual stress of U-rib stiffened plates. *J. Constr. Steel Res.* **2020**, *175*, 106362. [CrossRef]
33. Zhang, Q.H.; Ma, Y.; Cui, C.; Chai, X.Y.; Han, S.H. Experimental investigation and numerical simulation on welding residual stress of innovative double-side welded rib-to-deck joints of orthotropic steel decks. *J. Constr. Steel Res.* **2021**, *179*, 106544. [CrossRef]